Polym. Bull. (2011) 67:1539–1551
DOI 10.1007/s00289-011-0495-y

ORIGINAL PAPER

The influence of temperature and interface strength on the microstructure and performance of sol–gel silica–epoxy nanocomposites

Tanzeela Nazir · Adeel Afzal · Humaira M. Siddiqi · Shaukat Saeed · Michel Dumon

Received: 26 October 2010 / Accepted: 25 April 2011 / Published online: 5 May 2011

Abstract A series of silica–epoxy nanocomposites were prepared by hydrolysis of tetraethoxysilane within the organic matrix at different processing temperatures, i.e., 25 and 60 °C. Epoxy matrices reinforced with 2.0–10.0 wt% silica were subsequently crosslinked with an aliphatic diamine hardener to give optically transparent nanocomposite films. Interphase connections between silica networks and organic matrix were established by in situ functionalization of silica with 2.0 wt% γ-aminopropyltriethoxysilane (APTS). The microstructure of silica–epoxy nanocomposites as studied by transmission electron microscopy indicated the formation of very well-matched nanocomposites with homogeneous distribution of silica at relatively higher temperatures and in the presence of APTS. Thermogravimetric and static mechanical analyses confirmed considerable increase in thermal stability, stiffness, and toughness of the modified composite materials as compared to neat epoxy polymer and unmodified silica–epoxy nanocomposites. A slight improvement in the glass transition temperatures was also recorded by differential scanning calorimetry measurements. High temperature of hydrolysis during the in situ sol–gel

T. Nazir · A. Afzal · H. M. Siddiqi (✉)
Department of Chemistry, Quaid-i-Azam University, Islamabad 45320, Pakistan
e-mail: humairas@qau.edu.pk

S. Saeed
Department of Chemical and Materials Engineering, Pakistan Institute of Engineering and Applied Sciences, Islamabad 45650, Pakistan

M. Dumon
Laboratoire des Matériaux Macrolmoléculaires, Institut National des Sciences Appliquées de Lyon, 69100 Villeurbanne Cedex, France

Present Address:
M. Dumon
Département Science et Génie des Matériaux, Institut Universitaire de Technologie, Université Bordeaux 1, 33405 Talence Cedex, France

process not only improved reaction kinetics but also promoted mutual solubility of the two phases, and consequently enhanced the interface strength. In addition, APTS influenced the size and distribution of the inorganic domain and resulted in better performance of the modified silica–epoxy nanocomposites.

Keywords Polymer composites · Thermosetting resins · Thermal properties · Mechanical properties

Introduction

Epoxy-based thermosetting resins are frequently used as advance composite matrices due to their extraordinary properties such as higher strength and stability, better adhesion, resistance to solvents, scratch and corrosion, and lower flammability [1–6]. These unique physical properties of epoxy resins insure their employment in numerous applications at the industrial and commercial scale. However, epoxy-based matrix materials usually decompose at elevated temperatures and are often brittle, which has prompted scientists and engineers to integrate a variety of hard materials such as inorganic glasses, clay, carbon nanotubes, etc., [7–10] to better thermal stability and toughness of resins. Relevant literature suggests that inorganic glass, i.e., silica derived from different sources, and through different mechanisms is an effective reinforcement for epoxy resin [7, 8, 11–14]. Silica–epoxy resin particulate or bicontinuous nanocomposites, for instance, have been prepared by dispersing preformed nanoscale silica powders in the resin matrix [15–18] or produced by in situ hydrolysis of different silane precursors and functionalized oligomers [12, 19]; and a significant increase in thermo-mechanical characteristics was recorded along with several other property benefits.

The sol–gel process [20–22] is extremely useful for the synthesis of thermally and mechanically superior silica–epoxy nanocomposites as it allows extensive distribution of the as-synthesized silica networks within matrix. It is well-known that the eventual properties of composite materials depend largely on the nature, size, and distribution of inorganic particles at the nanoscale, and subsequently on the strength of interface [12, 13]. Where smaller and homogeneously distributed silica particles would add to the performance of composite materials, better adhesion between the organic and inorganic phases would exponentiate it. In this perspective, the sol–gel process promises particularly improved distribution and mixing of nanoscale silica in situ [21, 22]. On the other side, reports suggest that silica–epoxy interphase can be strengthened by suitable functionalization of the organic or inorganic monomers and by the use of an appropriate coupling reagent [23, 24].

In recent years, several workers exploited the sol–gel reaction either in one-step simultaneous or in two-step sequential procedure to produce sol–gel composite materials based on epoxy resins [19–23, 25]. Recently we have employed a tailored approach to synthesize sol–gel hybrids based on epoxy resins with very fine interface regions and superior thermal and mechanical properties [26]. In view of the fact that different processing conditions such as temperature changes strongly influence the ultimate performance of nanocomposites even if they are based on

similar silica/matrix ratios; we hereby present a chronological study of this focus, which is up till now unclear albeit huge flux of research in the area of in situ sol–gel derived composite systems. For this reason, a series of different silica–epoxy nanocomposites are developed to study (a) the effect of different processing temperatures on the composite microstructure, (b) the evolution of interfacial interactions at different temperatures, and (c) how it affects the eventual performance of composites in terms of their thermal and mechanical behavior. The processing temperature in this case means the temperature at which hydrolysis and polycondensation of different alkoxysilane precursors was carried out within the epoxy resin; and is different from the curing temperature.

Experimental

Materials

The organic matrix was composed of epoxy and amine precursors, i.e., diglycidyl ether of bisphenol A, DGEBA (Epoxy equivalent = 174.2 g/mol) and Jeffamine D-400 (NH equivalent = 99.7 g/mol), respectively obtained from DOW Chemicals and Huntsman. The inorganic component was constituted of SiO_2 network derived from the hydrolysis and condensation of tetraethylorthosilicate (TEOS). The in situ functionalization of the silica was achieved by hydrolysis and crosslinking of γ-aminopropyltriethyoxysilane (APTS). TEOS and APTS were received from HULS America Inc. and ABCR Germany, respectively and were used as received.

Synthesis

A series of silica–epoxy nanocomposites, namely; SE, SE†, and SE‡ nanocomposites, are prepared by integrating 2.0–10.0 wt% silica in the epoxy–amine matrix. The SE series symbolizes the un-modified silica–epoxy nanocomposites processed at 25 °C, while SE† and SE‡ series represent modified or in situ functionalized silica–epoxy nanocomposites processed at 25 and 60 °C, respectively. Table 1 indicates the types of nanocomposites synthesized along with the nomenclature, sample composition, and the temperature at which hydrolysis and condensation of TEOS was performed. A neat epoxy polymer cured with diamine is also prepared by mixing stoichiometric amounts of epoxy and amine monomers, i.e., DGEBA:D-400 = 2:1. Neat polymer film is produced by casting the mixture on glass plates pre-coated with Teflon and curing it for 5 h at 100 °C.

Synthesis of different types of silica–epoxy nanocomposites was carried out by pre-polymerizing silanes with water in the presence of calculated amounts of DGEBA to achieve finer distribution of inorganic network within epoxy–resin, which was then cured with Jeffamine D-400. The detailed method is described elsewhere [26]. In brief, epoxy resin was mixed with different amount of silane precursors in a stepwise process and stirred vigorously for 2 h after each step under anhydrous conditions. The stoichiometric amount of water was added to the reaction mixture, and it was stirred for 4 h to properly hydrolyze silanes. To prepare SE† and

Table 1 Composition of different silica–epoxy composite materials

Types of materials synthesized	Sample ID	Amount of SiO_2 (wt%)				Processing temperature (°C)
		From TEOS	From APTS	Total[a] (calc.)	Total[b] (formed)	
Neat epoxy polymer	SE0	0.0	0.0	0.0	0.0	–
Silica–epoxy nanocomposites						
SE series	SE2	2.0	0.0	2.0	1.75 ± 0.05	25
	SE5	5.0	0.0	5.0	4.49 ± 0.08	
	SE7	7.0	0.0	7.0	6.28 ± 0.10	
	SE10	10.0	0.0	10.0	8.86 ± 0.15	
SE† series	SE†2	1.96	0.04	2.0	1.87 ± 0.03	25
	SE†5	4.90	0.10	5.0	4.72 ± 0.05	
	SE†7	6.86	0.14	7.0	6.62 ± 0.07	
	SE†10	9.80	0.20	10.0	9.40 ± 0.06	
SE‡ series	SE‡2	1.96	0.04	2.0	1.95 ± 0.02	60
	SE‡5	4.90	0.10	5.0	4.91 ± 0.04	
	SE‡7	6.86	0.14	7.0	6.87 ± 0.05	
	SE‡10	9.80	0.20	10.0	9.85 ± 0.06	

[a] Amount of silica theoretically calculated from the reaction stoichiometry

[b] Amount of silica actually formed, experimentally calculated by burning at least three samples at 1000 °C in air

SE‡ nanocomposites, APTS and TEOS in a ratio of 1: 49 were pre-hydrolyzed at 25 and 60 °C, respectively. Finally calculated amount of diamine was added to crosslink epoxide groups in the organic matrix holding SiO_2 networks, and the mixture was cured for 5 h at 100 °C. Depending upon the composition of the nanocomposites (see Table 1); the reagents were mixed in following ratios: (DGEBA:D-400 = 2:1, TEOS:Water = 3:1, APTS:Water = 2.25:1, and TEOS: APTS = 49:1).

Instruments

Fourier transform infrared (FTIR) spectra of free standing composite films were obtained through Perkin Elmer system 2000 FTIR spectrophotometer. For microscopic characterization, samples were first microtomed with a diamond knife on a Leica EMFCS instrument at −50 °C to give sections with a nominal thickness of 80 nm, deposited on Cu grids and then imaged with a Philips CM 120 Transmission Electron Microscope (TEM) at an operating voltage of 100 kV. The contrast between silica and epoxy phases was sufficient for imaging; therefore no staining was required [27].

Thermal degradation of the nanocomposites was studied using Perkin Elmer TGA-7 analyzer in the presence of air. The samples were heated to 800 °C at a rate of 10 °C/min. Differential scanning calorimetry (DSC) of the cured samples was

performed with a Perkin Elmer DSC-7 Instrument by heating the sample from −20 to 310 °C at a constant heating rate of 10 °C/min under inert (N_2) atmosphere.

Static mechanical analysis was performed on samples with dimensions (ca. 15.0 × 5.0 × 0.15–0.20) mm. They were vacuum dried at 70 °C for 5 h before analysis. Stress–strain responses were measured with Testometric Universal Testing Machine M350/500 manufactured by Testometric UK, with a cross head speed of 5 mm/min. The measurements were performed at 25 °C and the average values obtained from at least six specimens are reported.

Results and discussion

Characterization

Silica–epoxy nanocomposites were initially characterized through FTIR spectroscopy for the presence of inorganic and organic networks. The formation of SiO_2 networks was verified by the characteristic absorption peak for Si–O–Si asymmetric stretching at 1090 cm^{-1}, as shown in Fig. 1. The absorption peak at 1180 cm^{-1} was attributed to C–N–C stretching of tertiary amines thereby confirming the formation of three dimensional epoxy–amine network. The fact was also supported by the absence of symmetric and asymmetric stretching of epoxide at 863 and 910 cm^{-1}, respectively [18, 28]. FTIR spectroscopy is a good tool for initial characterization of thin films and it gives significant information about the formation of SiO_2 networks and the completion of crosslinking reaction. However, the complex nature of the nanocomposites and presence of like bonds in different series of composite materials made it difficult to distinguish between them through their FTIR spectra.

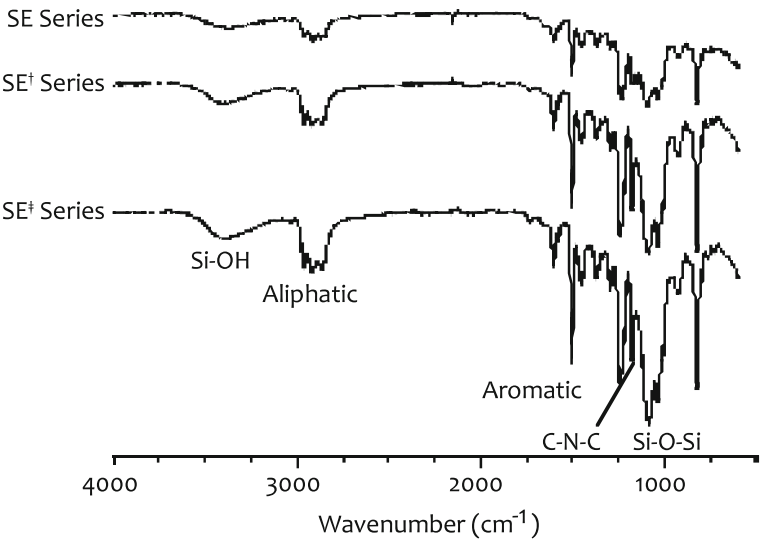

Fig. 1 FTIR spectra of different types of silica–epoxy composite films with 5 wt% silica

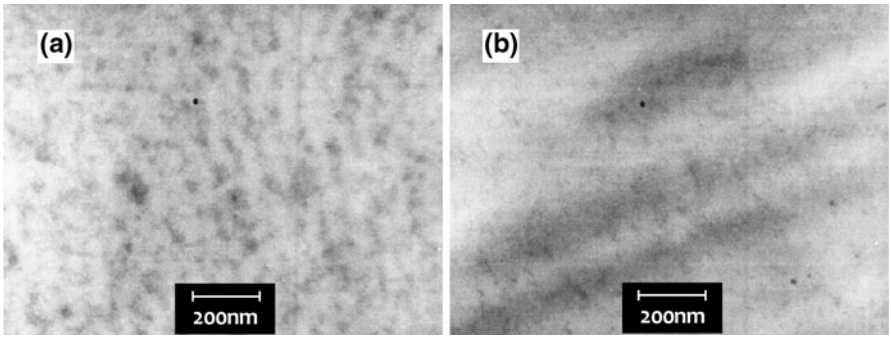

Fig. 2 TEM images showing the morphology of **a** SE10 and **b** SE†10 nanocomposite thin films with 10 wt% silica

The morphology of various materials analyzed by TEM, however, evidently makes a distinction between the samples from different series of nanocomposites. Figure 2 displays the TEM images of SE10 and SE†10 nanocomposites; where silica content is same (10 wt%) but the two films differ in absence or presence of APTS, respectively. The existence of bi-phase morphology was clearly represented in SE10 thin film (see Fig. 2a), which consisted of hyper-branched silica clusters dispersed in the epoxy resin matrix. The size of silica clusters ranges between 80 and 120 nm. In case of SE†10, however, rather homogeneous distribution of silica networks in the matrix can be seen owing to the presence of APTS (see Fig. 2b). Hence, minor amounts (only 2 wt% of the total inorganic content) of the coupling agent affect the overall morphology of the nanocomposites by promoting miscibility of the two phases, and effectively by reducing the size of silica clusters.

One of the most important aspects of this study was to determine the influence of temperature changes on the sol–gel process and the morphology of resulting composites. The effect of temperature on size and distribution of silica particles can clearly be observed, for example, by comparing the morphology of SE†7 and SE‡7 thin film nanocomposites; as both contain similar amounts of silica (7.0 wt%) but processed at different temperatures, 25 and 60 °C, respectively. Figure 3 shows the TEM images of these films.

Even though, the micrographs in Fig. 3 show very fine distribution of nanoscale silica in the organic matrix attributed to the presence of APTS; the inorganic phase in SE‡7 nanocomposite film appears to be rather dense and with most likely the finest distribution of inorganic networks in the matrix (see Fig. 3b). A profound change in behavior was not predicted since increase in temperature had only been reported to decreases the time required to reach sufficient viscosity, and accelerate the hydrolysis–condensation process [29]. Nonetheless, higher processing temperature enhanced the mutual solubility of the constituents simultaneously, and further suppressed the microscopic phase separation tendency in SE‡ series composites. The strength of interphase was increased as a consequence of superior miscibility of the constituents at elevated processing temperature, thus resulting in morphologically better nanocomposites.

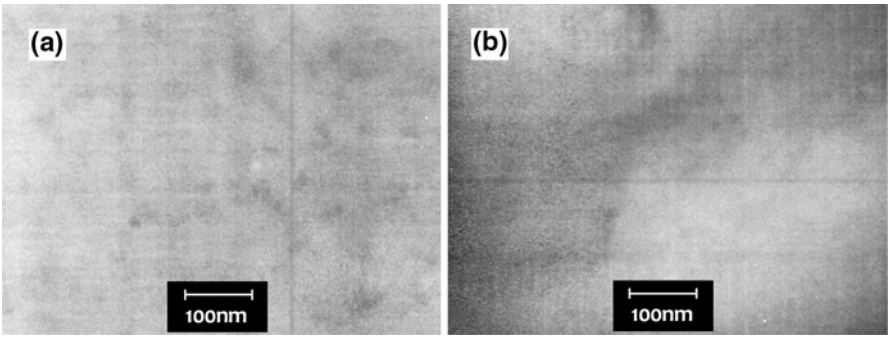

Fig. 3 TEM images of **a** $SE^{\dagger}7$ and **b** $SE^{\ddagger}7$ nanocomposite thin films with 7 wt% silica

Thermal properties

The silica–epoxy nanocomposites were tested by TGA in oxygen atmosphere to study the effect of sol–gel derived silica on their thermal degradation and stability at elevated temperatures. Figure 4 shows TGA thermograms of the nanocomposite samples reinforced with 2.0, 5.0, 7.0, and 10.0 wt% silica. Thermal decomposition of the neat epoxy polymer exhibits a single step degradation with T_{max} just above 550 °C. In the presence of nanosilica, a two-step degradation profile was observed for nanocomposites with significant increase in degradation temperatures as compared to the neat epoxy polymer. The increase in thermal decomposition temperatures, e.g., at 10 and 50% and maximum weight loss was linear and gradual with respect to silica loadings. This suggests improved thermal stability and better performance of the nanocomposites at higher temperatures. The existence of silica network is responsible for reduced rate of degradation in all silica–epoxy composite systems. In $SE^{\dagger}$ and $SE^{\ddagger}$ nanocomposites, however, interactions between the inorganic and organic components further restrict thermal degradation of macromolecular chains; hence the onset of thermal degradation temperatures in $SE^{\dagger}$ and $SE^{\ddagger}$ nanocomposites is shifted to relatively higher temperatures with reference to the neat epoxy polymer and SE nanocomposites.

The ceramic/char yield obtained from the respective TGA thermograms and by heating at least three samples to 1000 °C in air provides further evidence of the greater amplitude of thermal stability of the $SE^{\dagger}$ and $SE^{\ddagger}$ nanocomposites. As shown in Table 1, the amount of residue for different series of nanocomposites increases in the following order: $SE < SE^{\dagger} < SE^{\ddagger}$ nanocomposites. It indicates that percent conversion of the individual silane precursors to silica networks increases from $88.9 < 94.1 < 98.0\%$ for these systems, respectively. These results also suggest that hydrolysis of silane precursors can be carried out successfully within the epoxy resin matrix in the absence of any external catalyst at slightly higher temperature. In case of $SE^{\ddagger}$ nanocomposites, higher temperature of hydrolysis further promotes the speed of sol gel reaction by reducing the colloidal time. On the other side, however, sol–gel reaction time (that was 4 h in all of the experiments) should be increased in order to optimize the conditions and to obtain 100% conversion of silane precursors.

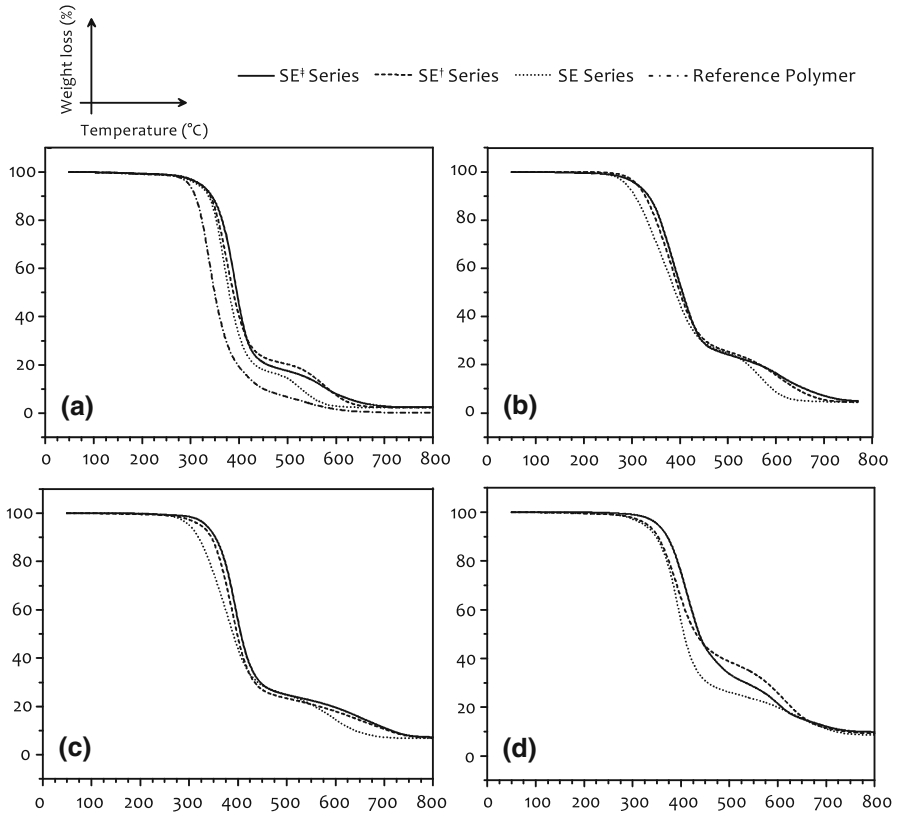

Fig. 4 TGA curves for various silica–epoxy nanocomposites with **a** 2.0 wt%, **b** 5.0 wt%, **c** 7.0 wt%, and **d** 10.0 wt% silica loadings

Nevertheless, due to better yield of SiO_2 networks at 60 °C, $SE^{\ddagger}$ series nanocomposites show greater extent of thermal stability.

DSC was used to determine the glass transition temperature (T_g) of various silica–epoxy composite materials. Figure 5 illustrates T_g of different series of nanocomposites with reference to the neat epoxy polymer. SE series composites show a small decrease in T_g, which is usually attributed to the decrease in polymer crosslinking density. Similar results have already been reported by various authors [30, 31]. However, contrary to their findings, T_g increases when APTS is introduced into the composite systems (i.e., in $SE^{\dagger}$ and $SE^{\ddagger}$ series). It was evident that T_g of these materials shifted to higher temperature with the increase in silica content attributed to the presence of coupling agent.

As previously observed by TEM, the use of APTS brings about the formation of denser networks in both constituent phases, and that is manifest through an increase in T_g. Prezzi and Mascia [23] reported a huge increase in T_g of silica–epoxy hybrids, while using the coupling agents with basic character. In the experiments, however, a maximum of 8.5% increase in T_g was observed for $SE^{\ddagger}5$ nanocomposite attributed

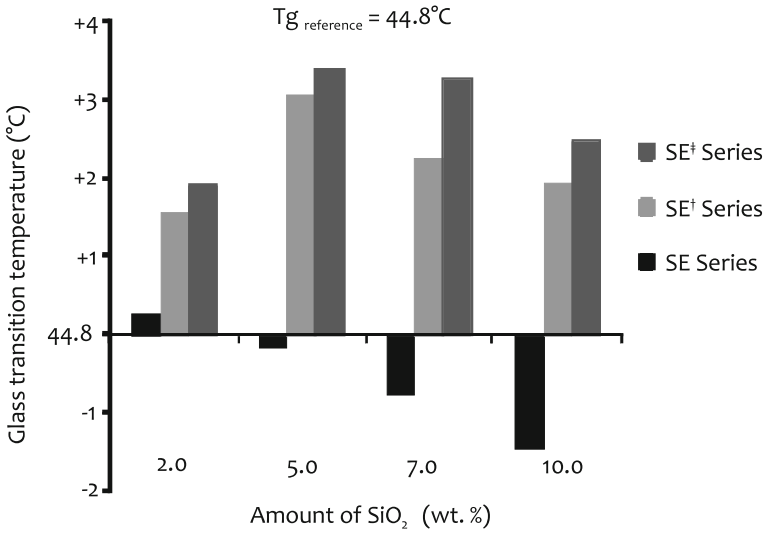

Fig. 5 Glass transition temperature (T_g) of the silica–epoxy nanocomposites with reference to the neat epoxy polymer

to relatively little amount of APTS used (only 2.0 wt% of total SiO_2). As the amount of silica increases above 5.0 wt%, however, a small drop in T_g values was also observed; suggesting reversal of the constructive effects of filler at higher loadings. Chen et al. [32] found that T_g of the samples decreased significantly beyond 5 wt% nanosilica loadings. Apparently it was unclear, why the decrease in T_g was only observed beyond a critical level, for example, 5 wt% SiO_2. However, in view of preceding results and interpretations [23, 32, and present study], it is assumed that a supplementary increase in the amount of APTS might diminish this problem at higher concentrations of fillers.

Mechanical properties

Mechanical properties of the neat epoxy polymer and different nanocomposite films were calculated from their stress–strain characteristics, and the data are recorded in Table 2. A monotonic increase in tensile strength and stiffness of the composite systems was observed with increasing silica loadings. The amplitude of increase in strength and modulus is greater in the in situ functionalized $SE^{\dagger}$ and $SE^{\ddagger}$ nanocomposites as compared to unmodified SE series. Mechanical properties of the nanocomposites certainly depend on the strength of interphase between the SiO_2 network and the organic matrix [33, 34]; and this is evidently reflected in the study. $SE^{\dagger}$ and $SE^{\ddagger}$ series nanocomposites exhibit larger increase in tensile properties due to phase interlinking through covalent bonds. SE series also shows a steady improvement in tensile strength, however, the elongation at break is notably reduced. It is drastically decreased for SE10 nanocomposites, which represents that the matrix starts to develop into a brittle one at higher SiO_2 loadings. These effects

Table 2 Mechanical properties of neat epoxy polymer and nanocomposite silica–epoxy thin films

Sample ID	Tensile strength (MPa)		Tensile modulus (GPa)		Strain at break (%)	
	σ	Dev.	E	Dev.	E	Dev.
SE0	20.2	0.7	4.17	0.07	71.1	1.9
SE2	22.5	0.5	4.36	0.07	68.8	2.1
SE5	24.7	1.0	4.99	0.12	65.9	2.1
SE7	26.3	0.9	5.70	0.09	61.6	2.4
SE10	29.0	1.0	6.73	0.13	57.5	2.5
SE†2	23.6	0.4	4.40	0.06	71.6	2.4
SE†5	27.1	0.9	5.14	0.09	70.3	1.8
SE†7	30.7	1.3	6.19	0.15	66.5	2.5
SE†10	34.8	1.2	7.37	0.15	63.0	2.0
SE‡2	24.4	0.6	4.53	0.08	71.8	2.2
SE‡5	28.8	1.2	5.31	0.17	72.4	1.6
SE‡7	32.6	0.8	6.41	0.12	67.9	2.1
SE‡10	37.7	1.1	7.76	0.16	64.7	2.3

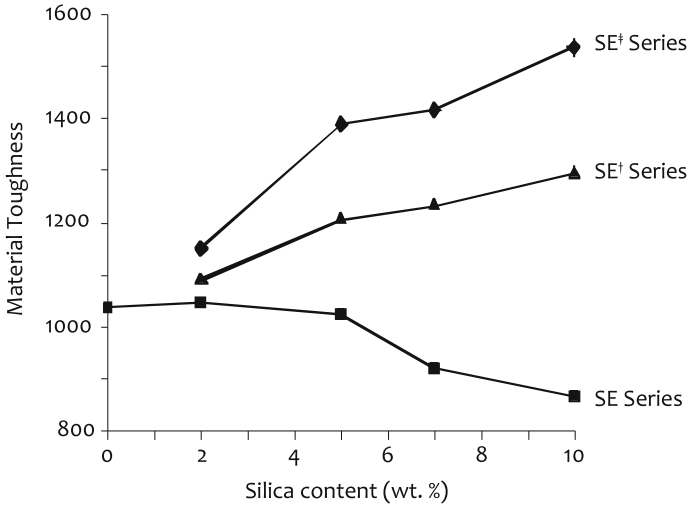

Fig. 6 Material toughness of the neat epoxy polymer and silica–epoxy nanocomposite materials as a function of silica loadings

were also manifest through comparison of the material toughness values obtained from the area of the stress–strain curves of various nanocomposite materials (see Fig. 6).

The observed decrease in strain at break and the material toughness of SE nanocomposite above 5 wt% are indicative of matrix brittleness at higher

concentrations of filler. Chen et al. [32] associated this phenomenon to a difference in resin properties that is either a decrease in T_g or a decrease in coupling between the particles and matrix.

A decrease in T_g may indicate the regions of lower crosslink density and the existence of low-energy paths around particles, which consequently result in reduced material toughness and elongation at break. However, a decrease in particle–matrix interactions seems more plausible, as increasing interfacial interactions through chemical bonding in SE† and chemical bonding plus elevated processing temperature in SE‡ series result in sufficient increase in toughness. Thus, we conclude that simultaneous improvements in stiffness and toughness might be obtained in the presence of a suitable coupling agent and relatively higher temperatures of hydrolysis for sol–gel derived silica–epoxy nanocomposites. The smaller, well-dispersed and well-matched filler particles efficiently dissipate the fracture energy, and result in matrix stiffness and toughening.

Conclusion

Different types of sol–gel silica–epoxy nanocomposites are produced by introducing nanosilica in the organic matrix through a tailored process, and their performance is evaluated in order to study the effect of processing temperature and interface strength. The analyses suggest that the nanocomposites have appreciably better thermal and mechanical characteristics as compared to the neat polymer. The in situ functionalization of silica with APTS improves the properties of cured silica–epoxy nanocomposites by developing interface interactions. Higher temperature during the sol–gel process remarkably influences the colloidal time by accelerating the speed of hydrolysis, affects the overall miscibility of constituents by progressive mixing, and avoids segregation of phases in addition. Thus, systems with covalently linked interface and processed at slightly higher temperatures signify the formation of substantially dense silica networks with drastically finer phase separated domains and better performance.

Acknowledgments Financial support by the University Research Fund, Quaid-i-Azam University, Islamabad is gratefully acknowledged.

References

1. Kwon SC, Adachi T, Araki W, Yamaji A (2008) Effect of composing particles of two sizes on mechanical properties of spherical silica–particulate-reinforced epoxy composites. Composites B 39:740–746
2. Liu YL, Wei WL, Hsu KY, Ho WH (2004) Thermal stability of epoxy–silica composite materials by thermogravimetric analysis. Thermochim Acta 412:139–147
3. Chang KC, Lin HF, Lin CY, Kuo TH, Huang HH, Hsu SC, Yeh JM, Yang JC, Yu YH (2008) Effect of amino-modified silica nanoparticles on the corrosion protection properties of epoxy resin–silica hybrid materials. J Nanosci Nanotechnol 8:3040–3049
4. Yu D, Liu W, Liu Y (2008) Study on heat resistance and flame retardation of polyfunctional epoxy–silica–phosphorus hybrid resins. Chem Lett 37:1118–1125

5. Cardiano P (2008) Hydrophobic properties of new epoxy–silica hybrids. J Appl Polym Sci 108:3380–3387
6. Chen S, You B, Zhou S, Wu L (2009) Preparation and characterization of scratch and mar resistant waterborne epoxy/silica nanocomposite clearcoat. J Appl Polym Sci 112:3634–3639
7. Davis SR, Brough AR, Atkinson A (2003) Formation of silica/epoxy composite network polymers. J Non-Cryst Solids 315:197–205
8. Xiao F, Sun Y, Xiu Y, Wong CP (2007) Formation, thermal and mechanical properties of POSS epoxy composite composites. J Appl Polym Sci 104:2113–2121
9. Liu W, Hoa SV, Pugh M (2005) Organoclay-modified high performance epoxy nanocomposites. Compos Sci Technol 65:2364–2373
10. Bekyarova E, Thostenson ET, Yu A, Kim H, Gao J, Tang J, Hahn HT, Chou TW, Itkis ME, Haddon RC (2007) Multiscale carbon nanotube–carbon fiber reinforcement for advanced epoxy composites. Langmuir 23:3970–3974
11. Huang CJ, Fu SY, Zhang YH, Lauke B, Li LF, Ye L (2005) Cryogenic properties of SiO_2/epoxy nanocomposites. Cryogenics 45:450–454
12. Mascia L, Prezzi L, Haworth B (2006) Substantiating the role of phase bicontinuity and interfacial bonding in epoxy–silica nanocomposites. J Mater Sci 41:1145–1155
13. Macan J, Brnardic I, Orlic S, Ivankovic H, Ivankovic M (2006) Thermal degradation of epoxy–silica organic–inorganic composite materials. Polym Degrad Stab 91:122–127
14. Tarrio-Saavedra J, Lopez-Beceiro J, Naya S, Artiaga R (2008) Effect of silica content on thermal stability of fumed silica/epoxy composites. Polym Degrad Stab 93:2133–2137
15. Adachi T, Osaki M, Araki W, Kwon SC (2008) Fracture toughness of nano- and micro-spherical silica-particle-filled epoxy composites. Acta Mater 56:2101–2109
16. Jiao J, Sun X, Pinnavaia TJ (2009) Mesostructured silica for the reinforcement and toughening of rubbery and glassy epoxy polymers. Polymer 50:983–989
17. Bugnicourt E, Galy J, Gerard JF, Barthel H (2007) Effect of sub-micron silica fillers on the mechanical performances of epoxy-based composites. Polymer 48:1596–1605
18. Brus J, Spirkova M, Hlavata D, Strachota A (2004) Self-organisation, structure, dynamic properties, and surface morphology of silica/epoxy films as seen by solid-state NMR, SAXS, and AFM. Macromolecules 37:1346–1357
19. Matejka L, Dukh O, Kolarik J (2000) Synthesis and characterization of organic–inorganic nano-composites based on epoxy resin and 3-glycidoxypropyltrimethoxysilane. Polymer 41:1449–1459
20. Lu SR, Zhang HL, Zhao CX, Wang XY (2005) Preparation and characterization of epoxy–silica composite materials by the sol–gel process. J Mater Sci 40:1079–1085
21. Matejka L, Plestil J, Dusek K (1998) Structure evolution in epoxy silica nanocomposites: sol–gel process. J Non-Cryst Solids 226:114–121
22. Ochi M, Matsumura T (2005) Thermomechanical properties and phase structure of epoxy/silica nanohybrid materials constructed from a linear silicone oligomer. J Polym Sci B 43:1631–1639
23. Prezzi L, Mascia L (2005) Network density control in epoxy–silica nanocomposites by selective silane functionalization of precursors. Adv Polym Technol 24:91–102
24. Lu SR, Wei C, Yu JH, Yang XW, Jiang YM (2007) Preparation and characterization of epoxy nanocomposites by using PEO-grafted silica particles as modifiers. J Mater Sci 42:6708–6715
25. Matejka L, Dusek K, Plestil J, Kriz J, Lednicky F (1999) Formation and structure of the epoxy–silica nanocomposites. Polymer 40:171–181
26. Nazir T, Afzal A, Siddiqi HM, Ahmad Z, Dumon M (2010) Thermally and mechanically superior hybrid epoxy–silica polymer films via sol–gel method. Prog Org Coat 69:100–106
27. Jackson CL, Bauer BJ, Nakatani AI, Barnes JD (1996) Synthesis of hybrid organic–inorganic materials from interpenetrating polymer network chemistry. Chem Mater 8:727–733
28. Ochi M, Takahashi R, Terauchi A (2001) Phase structure and mechanical and adhesion properties of epoxy/silica nanocomposites. Polymer 42:5151–5158
29. Gu JW, Zhang QY, Li HC, Tang YS, Kong J, Dang J (2007) Study on preparation of SiO_2/epoxy resin hybrid materials by means of sol–gel. Polym Plast Technol Eng 46:1129–1134
30. Mahrholz T, Stangle J, Sinapius M (2009) Quantitation of the reinforcement effect of silica nanoparticles in epoxy resins used in liquid composite molding processes. Composites A 40: 235–243
31. Sun YY, Zhang ZQ, Moon KS, Wong CP (2004) Glass transition and relaxation behavior of epoxy nanocomposites. J Polym Sci B 42:3849–3858

32. Chen C, Justice RS, Schaefer DW, Baur JW (2008) Highly dispersed nanosilica–epoxy resins with enhanced mechanical properties. Polymer 49:3805–3815
33. Tjong SC (2006) Structure and mechanical properties of polymer nanocomposites. Mater Sci Eng R 53:73–197
34. Zhao Q, Hoa SV (2007) Toughening mechanism of epoxy resin with micro/nanoparticles. J Compos Mater 41:201–219